Research
Unconventional and Intelligent Oil & Gas Engineering—Article

# Direct Evidence of Coal Swelling and Shrinkage with Injecting $CO_2$ and $N_2$ Using *in-situ* Synchrotron X-ray Microtomography

Guanglei Zhang [a], P.G. Ranjith [b,*], Herbert E. Huppert [c]

[a] *Department of Earth Science and Engineering, Imperial College London, London SW7 2BP, UK*
[b] *Deep Earth Energy Laboratory, Department of Civil Engineering, Monash University, Melbourne, VIC, 3800, Australia*
[c] *Institute of Theoretical Geophysics, King's College, Cambridge CB2 1ST, UK*

A B S T R A C T

Deep coal seams are one of the world's most widespread deposits for carbon dioxide ($CO_2$) disposal and are generally located near large point sources of $CO_2$ emissions. The injection of $CO_2$ into coal seams has great potential to sequester $CO_2$ while simultaneously enhancing coalbed methane ($CO_2$-ECBM) recovery. Pilot tests of $CO_2$-ECBM have been conducted in coal seams worldwide with favorable early results. However, one of the main technical barriers in coal seams needs to be resolved: Injecting $CO_2$ reduces coal permeability and well injectivity. Here, using *in situ* synchrotron X-ray microtomography, we provide the first observational evidence that injecting nitrogen ($N_2$) can reverse much of this lost permeability by reopening fractures that have closed due to coal swelling induced by $CO_2$ adsorption. Our findings support the notion that injecting minimally treated flue gas—a mixture of mainly $N_2$ and $CO_2$—is an attractive alternative for ECBM recovery instead of pure $CO_2$ injection in deep coal seams. Firstly, flue gas produced by power plants could be directly injected after particulate removal, thus avoiding high $CO_2$-separation costs. Secondly, the presence of $N_2$ makes it possible to maintain a sufficiently high level of coal permeability. These results suggest that flue-gas ECBM for deep coal seams may provide a promising path toward net-zero emissions from coal mines.

© 2022 THE AUTHORS. Published by Elsevier LTD on behalf of Chinese Academy of Engineering and Higher Education Press Limited Company. This is an open access article under the CC BY-NC-ND license (http://creativecommons.org/licenses/by-nc-nd/4.0/).

## 1. Introduction

Anthropogenic energy-related carbon dioxide ($CO_2$) emissions are higher than ever and continue to increase [1]. The Intergovernmental Panel on Climate Change (IPCC) highlights the necessity of restricting global temperature rise to within 1.5 °C above pre-industrial levels, which requires reducing 45% of $CO_2$ emissions by 2030 and reaching net zero around 2050 [2]. A solution to the current problem is to capture $CO_2$ from anthropogenic sources and safely store it in the deep subsurface for geological lengths of time [3–7]. The process of carbon capture and storage (CCS) could contribute one-sixth of the required reduction of $CO_2$ emissions into the atmosphere by 2050 [8]. Thus, this technology could play an important role in large-scale $CO_2$ reduction [9], providing a bridging solution during the transitional period of the next few decades, during which we will continue to rely on fossil energy until the world energy system has time to move toward a lower carbon, long-term future.

Carbon dioxide enhanced oil recovery ($CO_2$-EOR) has been successfully developed and applied in the oil and gas industry for decades [10]. The new concept and technology of storage-driven $CO_2$-EOR, which was developed by Liu et al. [11,12], is able to achieve net-zero $CO_2$ emission while accomplishing maximum oil recovery in oilfields, which significantly reduces $CO_2$ emission and increases the economic benefit of CCS. Similarly, the storage of $CO_2$ in deep coal seams offers exceptional potential to achieve the "value-added" enhanced recovery of coalbed methane ($CH_4$) concurrently with carbon sequestration, in what is known as $CO_2$-enhanced coalbed methane ($CO_2$-ECBM) recovery [13,14]. The injected $CO_2$ is known to adsorb preferentially over $CH_4$ onto the surfaces of coal micropores [15]. From their proven records of $CH_4$ production, coal seams have long histories of both available storage capacity and long-term safety against gas escape. Although deep coal seams are estimated to have a relatively smaller capacity for $CO_2$ storage than saline aquifers (up to 10 000 Gt) and oil/gas fields (up to 900 Gt), their storage potential is still significant, at up to 200 Gt [5], compared with current anthropogenic $CO_2$ emissions of almost 40 Gt $CO_2$ annually. Moreover, coal seams are one of the world's most widespread deposits for $CO_2$ storage and are

generally located fairly near to large $CO_2$ emission sources, such as fossil-fueled power plants.

The concept of $CO_2$-ECBM in deep coal seams was in an embryonic stage from the 1970s [16] to the 1980s [17,18] in the laboratory, where pioneers found that $CO_2$ injection is capable of displacing the adsorbed $CH_4$ in coal. In the 1990s, the concept of ECBM recovery through displacement desorption using $CO_2$ was officially proposed [19]. Since then (1995–present), more than a dozen pilot projects in North America [19,20], Asia [21–23], and Europe [24] have demonstrated the feasibility of this technology in micro- to large-scale field tests, with the total amount of $CO_2$ injected ranging from 90 to 336 000 t [21]. The ongoing pilot testing worldwide shows favorable early results, with a potential to displace 95% of the original gas in place. However, implementation has been hampered by a technical challenge: Loss of coal permeability during $CO_2$ injection, especially near the wellbore region, has been reported to lead to a higher permeability reduction of over two orders of magnitude [21,22,24,25]. The swelling also creates a high stress zone near the wellbore region [22,26], and the injection pressure needed increases in order to maintain the injection rate. However, great care must be taken to avoid fracturing the caprock or re-activating faults through overpressure. The issue of reduced permeability and injectivity needs to be addressed before $CO_2$-ECBM can be deployed in deep coal seams on a large scale worldwide.

Acknowledging that several solutions have been adopted following field tests, including hydraulic fracturing and multiple-well injection [21,22], and that the challenges brought by these techniques include cost and environmental concerns, we need more economical and easier alternatives. Encouragingly, a recent field pilot in the Ishikari Coal Basin of Japan demonstrated that injecting pure nitrogen ($N_2$) over a period of days can reverse the reduced permeability caused by past $CO_2$ injections [22]. However, these results were inferred from strain or permeability measurements [27–30], rather than from direct observation of fracture networks using imaging methods under *in situ* conditions. This hypothesis has not yet been tested by directly observing the fracture network change caused by $CO_2/N_2$ injection.

Here, we prove this long-standing hypothesis by introducing a novel X-ray transparent triaxial core holder (Fig. 1; also see Refs. [31,32] for technical details) to conduct X-ray microtomography under *in situ* stress conditions, while simultaneously conducting core flooding tests. We operated the experiment in five stages (Fig. 2; see Section 2 for more details): ① the initial confined condition; ② pure $N_2$ injection; ③ pure $CO_2$ injection; ④ shut-in for $CO_2$ adsorption; and ⑤ a second pure $N_2$ injection. We conducted core flooding tests to quantify the permeability variations caused by injecting $N_2$, then $CO_2$, and then $N_2$ again. At the same time, we selected synchrotron X-ray phase-contrast microtomography as the best candidate for obtaining high spatial and time resolution X-ray images. Here, we provide direct observational evidence of fracture network changes.

## 2. Material and methods

### 2.1. Sample preparation

The sub-bituminous coal sample (Table 1) chosen for this study was collected from a coal seam buried at 400 m depth in the Datong coalfield in the Shanxi Province of China. The detailed geological conditions of the coal seam can be found elsewhere [33]. To
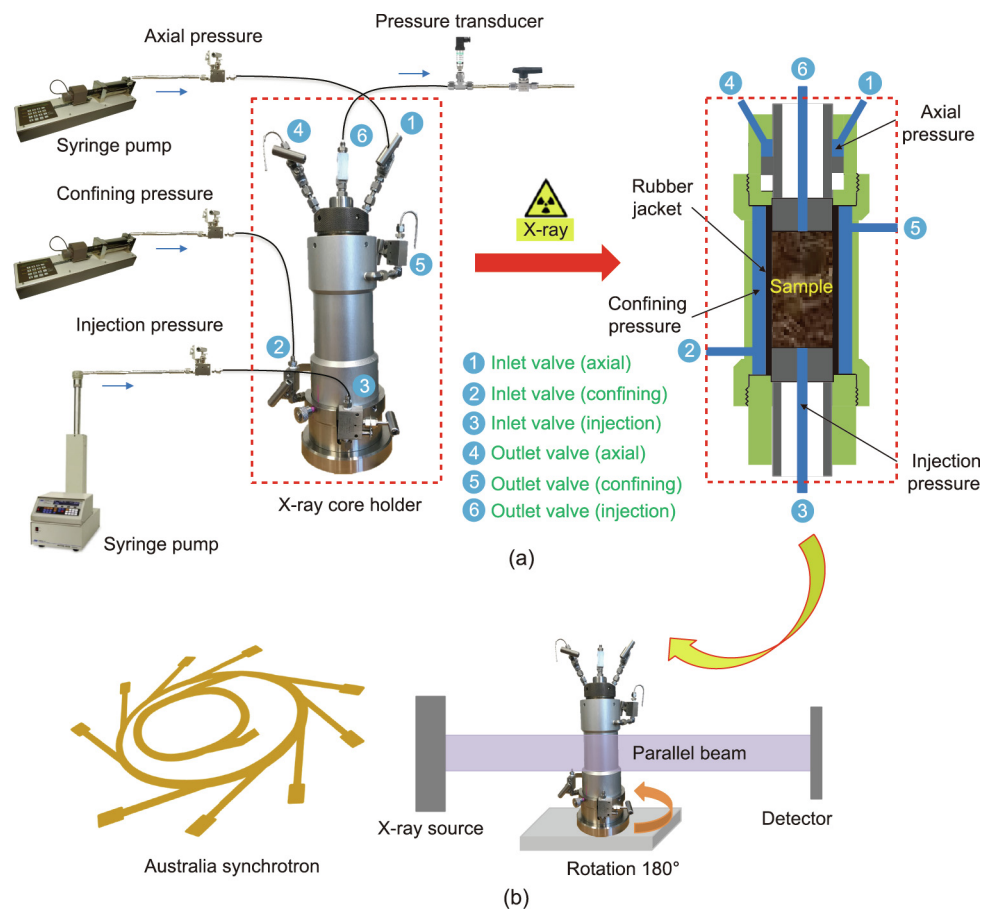


Fig. 1. (a) X-ray transparent triaxial core holder for the core flooding experiment with (b) X-ray microtomography.
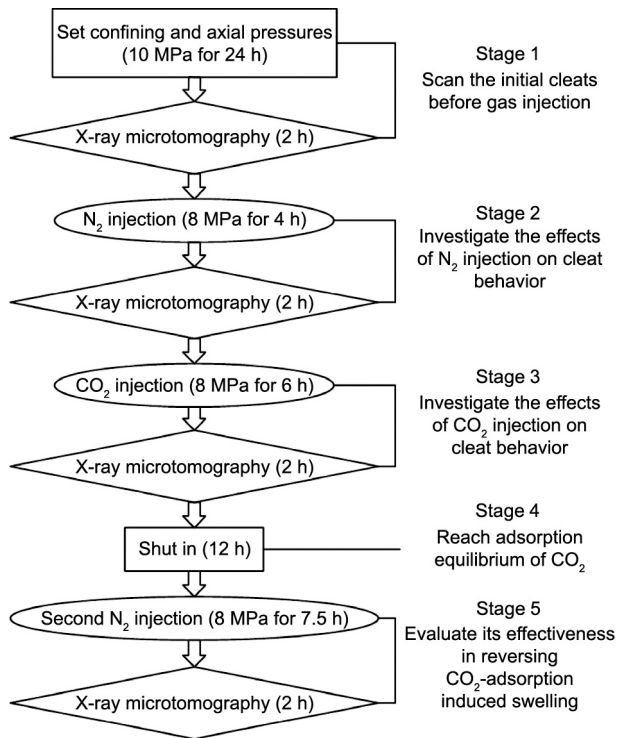
**Fig. 2.** A flow chart of the experimental procedures.

prevent the collected samples from further oxidizing and losing moisture, they were carefully wrapped with cling wrap before being transported to the laboratory; once there, they were kept in a fog room until testing. Since the objective of this study was to investigate the influence of fluid injection on coal fracture network change, it was necessary to select a naturally fractured coal sample. However, using a core barrel, it is easy to break core samples while drilling them from a coal block that contains natural fractures. Instead, we obtained a cylindrical sample with a diameter of 35 mm and a length of 70 mm through thread cutting.

### 2.2. Experimental procedures

We assembled the naturally fractured sub-bituminous coal into an X-ray transparent triaxial core holder (Fig. 1), then applied 10 MPa of confining and axial pressures to the sample. We scanned the sample to determine the initial conditions after the pressures were stabilized for 24 h. The sample was initially free of fluids; it was then sequentially saturated by $N_2$ (8 MPa), $CO_2$ (8 MPa), and $N_2$ (8 MPa) again. The optimum depth of coal seams for $CO_2$ sequestration is suggested to be 800–1000 m [34]. Therefore, fluid pressure of 8 MPa (about 800 m deep) was chosen by considering the hydrostatic pressure gradient of coal seams. We conducted all injections at room temperature (23 °C). This meant that the injected $CO_2$ was in liquid form, which is consistent with current technologies for most $CO_2$-ECBM sequestration projects in the field [21]. Pure $N_2$ was first injected for 4 h to estimate the initial

permeability of the coal sample. Subsequently, we injected pure $CO_2$ for 7 h to study the effect of $CO_2$ on coal permeability. After that, we closed both the upstream and downstream $CO_2$, so the pressurized $CO_2$ was maintained in the sample for 12 h. This process is called the "shut-in" period in field projects, allowing the injected $CO_2$ to be fully adsorbed into the coal [21]. Finally, we performed a second $N_2$ flooding to evaluate its effectiveness in improving the reduced permeability. The sample was computed tomography (CT) scanned after every injection (Fig. 2).

### 2.3. Permeability measurement

Although a coal sample with natural fractures was obtained for the permeability tests, the permeability of coal is very low, and it takes a long time to reach a steady flow. Since the adsorption of $CO_2$ onto coal is also a time-dependent process, it becomes necessary to determine permeability during a short time period in comparison with the adsorption time. In this study, the permeability of coal was measured using the pressure-transient method first developed by Brace et al. [35], which can determine the permeability of tight rocks fairly rapidly. The upstream pressure was maintained at 8 MPa and downstream pressure development (from 6 to 8 MPa) was monitored during the permeability test. The downstream pressure was released to 6 MPa after each permeability test and then increased to 8 MPa again during the subsequent permeability test. The logarithm of the differential pressure between upstream and downstream is plotted versus time in Fig. 3. The decay curve follows a linear function and can be fitted by the following equations [35,36]:

$$\Delta P(t) = \Delta P_0 e^{-\alpha t} \tag{1}$$

$$\alpha = \frac{kA}{\beta V_{down} L \mu} \tag{2}$$

where $\Delta P(t)$ is the pressure difference between the upstream and downstream pressure, $\Delta P_0$ is the pressure difference between
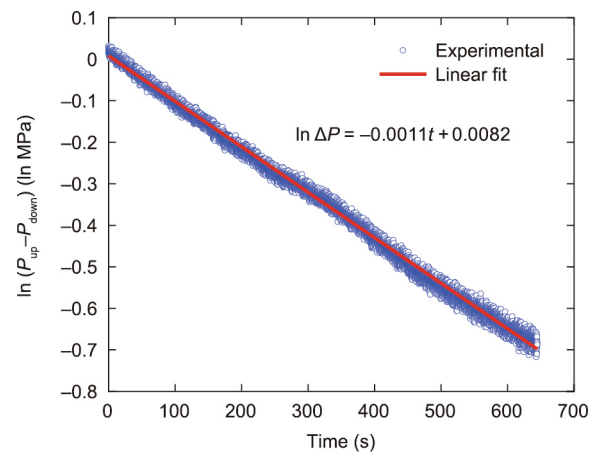


**Fig. 3.** Permeability measurement example showing the logarithmic decay curve of the pressure difference between upstream and downstream. $P_{up}$ is the upstream pressure and $P_{down}$ is the downstream pressure.

**Table 1**
Physical properties of the coal sample.

| Coal rank | $R_{o,m}$ | Proximate analysis (wt%) | | | Maceral groups (vol%) | | |
|---|---|---|---|---|---|---|---|
| | | $M_{ad}$ | $A_d$ | $V_{daf}$ | Vitrinite | Inertinite | Liptinite |
| Sub-bituminous | 0.46 | 2.00 | 23.05 | 25.86 | 46.9 | 48.8 | 4.3 |

$R_{o,m}$: maximum vitrinite reflectance under oil immersion; $M_{ad}$: moisture content (air-dried basis); $A_d$: ash yield (dry basis); $V_{daf}$: volatile matter content (dry, ash-free basis).

upstream and downstream at the initial stage, $t$ is time, $\alpha$ is the decay exponent (the slope of the line on the plot of ln ($\Delta P$)), $k$ is the permeability, $A$ is the cross-sectional area of the sample, $\beta$ is the compressibility of the fluid, $V_{down}$ is the volume of the downstream reservoir, $L$ is the sample length, and $\mu$ is the viscosity of the fluid.

### 2.4. In situ synchrotron X-ray phase-contrast microtomography

X-ray tomography using a monochromatic beam was carried out at hutch 3B of Australian Synchrotron's Imaging and Medical Beamline (IMBL). The detailed setup of the CT scanning system of IMBL can be found elsewhere [31,32]. Conventional absorption-based CT and phase-contrast CT share the same setup and image-collection procedures; however, the sample-to-detector distance is larger in the case of phase-contrast imaging. The Ruby detector (a PCO Edge camera lens coupled to a scintillator) was used for imaging the core holder with a sample-to-detector distance of 5 m, providing phase-contrast imaging to enhance the edges of different phases in the CT images. The scanning voltage was 65 keV, with a resolution of 14.6 μm. The tomographic scan comprised 1800 views of the sample over 180° rotation. Each view took 2 s for the X-ray exposure, and a total time of around 1 h was needed for the image acquisition. The Ruby camera has a complementary metal oxide semiconductor (CMOS) sensor with a pixel matrix of 2560 × 2160, coupled to an X-ray scintillator. The radiographic field of view was approximately 45 mm horizontally and 30 mm vertically. The vertical view was limited by the beam rather than the detector. Two vertical scans were conducted and stitched together to obtain an image of the sample that was 50 mm in height.

### 2.5. X-ray image processing

The projection X-ray images were first corrected using flat and dark signal images (ImageJ; National Institutes of Health, USA), and then reconstructed into slices using X-TRACT software [37] on the Australian Synchrotron Compute Infrastructure (ASCI) computing cluster. Analysis of the images was accomplished using Avizo standard software (version 9.5, Visualization Sciences Group). Grayscale CT images (Fig. 4) were first denoised using the non-local median filter and then segmented using a watershed segmentation algorithm. Technical details of the image processing and segmentation procedures can be found in Ref. [38]. Pore network models were then extracted from the segmented fracture networks using the Avizo software to quantify the pore-size distributions. As the

pore space in fracture networks is not spherical, an extension (i.e., a skeleton method) available in the software was used to provide a mode optimized for separating arbitrary pore shapes. The Avizo software incorporates the pore network modeling algorithm in Ref. [39], which consists of three main steps: ① pore space skeletonization, ② skeleton partitioning into groups, and ③ geometrical separation and labeling of pores.

## 3. Results and discussion

### 3.1. Permeability evolution during fluid injection

The permeability of the fractured coal sample (Fig. 5) did not change much with exposure time when we first injected $N_2$, which is a relatively inert gas. We did not expect significant swelling in this context, since the adsorption capacity of $N_2$ is generally far less than (about one-fourth) that of $CO_2$ [19]. However, when we used $CO_2$ as the injection fluid for 6 h, the coal sample's permeability significantly decreased (by an order of magnitude). The permeability decreased quickly for the first 2 h (falling by 70%), and then slowed until it reached a relatively constant value around 1 μD. This is because adsorption happened readily upon $CO_2$ injection, followed by a much slower diffusion of $CO_2$ into the coal. In addition, the fracture contact area increased in response to the increased swelling strain, resulting in a decrease of fracture compressibility. Hence, the permeability reduction became slower with exposure time.

Next, the permeability of the coal sample improved after being exposed to the second $N_2$ flooding. Swelling strain is directly related to the amount of $CO_2$ adsorption. $N_2$ injection helps to preserve permeability by lowering the partial pressure of $CO_2$ in the coal, which causes adsorbed $CO_2$ to desorb from the coal matrix. The permeability of the sample exposed to $N_2$ increased steadily by an order of magnitude from around 1 to 15 μD over 7.5 h of reinjection, and was eventually back to 30% of the initial level before $CO_2$ flooding. The permeability after the second $N_2$ flooding did not recover its original value before $CO_2$ injection. This seems to be consistent with other research, which found that a 25%–45% recovery rate can be achieved, depending on the $N_2$ flooding pressures and durations [29]. The extent of permeability reversal increases with increasing injection pressure and time, and decreases with an increase of overburden stresses [29]. In fact, after long exposure (18 h) to $CO_2$, including both $CO_2$ injection and shut-in periods, the desorption process from the coal matrix may take longer. On the other hand, this allows us to hypothesize that, after $CO_2$ is adsorbed for long enough, stronger chemical
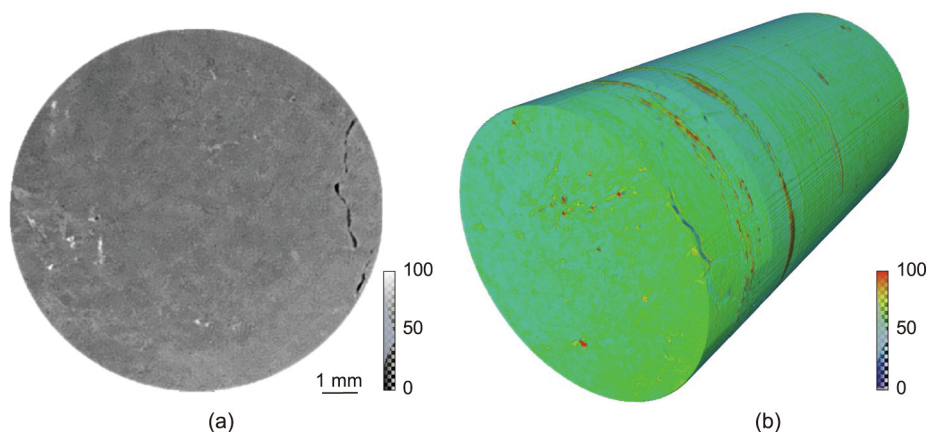


**Fig. 4.** X-ray CT image of the sample (obtained from stage 2). (a) Grayscale two dimensional (2D) CT image: minerals, organic matter, and fractures are shown in white, grey, and black, respectively, depending on the X-ray attenuation. (b) Three dimensional (3D) volume rendering of the sample: the colormap represents the relative X-ray intensities of various phases.
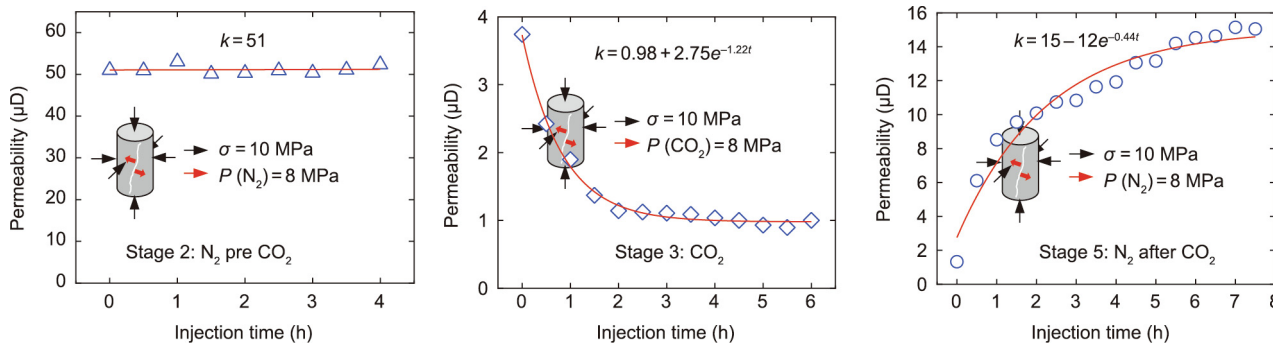
**Fig. 5.** Permeability changes at stages 2, 3, and 5 ($\sigma$: confining and axial pressures; $P$: fluid pressure).

adsorption of $CO_2$ into coal occurs, and the reversal from $N_2$ flooding cannot return the coal sample to its original condition.

### 3.2. Pore-scale mechanisms of permeability evolution

We observed the fracture network changes in a region of interest (10.5 mm in diameter and 18 mm long) at different injection stages (Figs. 6 and 7(a)). After stage 2 ($N_2$ injection for 4 h), fractures opened from their initial confined condition. This occurred because the decrease of effective stress from 10 to 2 MPa after fluid injection tended to mechanically open the fractures. The porosity increased by 67%, from 0.12% to 0.20%, after $N_2$ injection. However, the fractures narrowed down and even closed after stage 3 (injecting $CO_2$

for 6 h) due to the coal matrix swelling that accompanied $CO_2$ adsorption. Thus, we attribute the great permeability reduction discussed above to the fracture closure observed here. The fracture porosity significantly decreased, from 0.20% to 0.02%. In other words, $CO_2$ injection reduced the porosity by 83% compared with the initial condition. After stage 5 (reinjecting $N_2$ for 7.5 h), the fractures opened up again and the fracture porosity rebounded to 0.06%—50% of the initial condition. This reflects the fact that reinjecting $N_2$ caused $CO_2$ desorption and hence induced shrinkage of the coal matrix, allowing fractures to open up. In summary, we observed the first direct evidence of how injecting $CO_2/N_2$ into coal induces fracture network evolution due to swelling and shrinkage. The observed evolution of the fracture network is highly consistent with the change in the permeability of coal.

We generated pore network models (Fig. 7(b)) to represent the complex fracture network and to quantify the statistics of the pore space. The pore-size distributions (Fig. 8) show that pores with an equivalent radius below 40 μm were dominant in the fracture networks regardless of the fluid-saturation conditions, which indicates that the fracture apertures were mostly smaller than 40 μm. After injecting $N_2$ for 4 h, the average pore size did not show significant changes; however, the number of pores increased from about 11 300 to about 15 000 (Table 2). Along with the greater number of pores, the percentage of well-connected larger pores (with a radius above 100 μm) increased from 41.7% to 55.2% after $N_2$ injection, which increased the connectivity of the flow path (Fig. 7(b) and Table 2). After injecting $CO_2$ for 6 h, the average pore size fell from 20.2 to 18.2 μm, and the number of pores decreased greatly to 4194. Moreover, the percentage of larger pores significantly decreased to 7.1%, reducing the connectivity of the fracture network. After reinjecting $N_2$ for 7.5 h, the average pore size increased back to 21.6 μm and the pore number rebounded to 5980. Meanwhile, the percentage of larger pores reversed to 22.2%. These findings reflect the fracture closure and the reduced fracture porosity and connectivity due to $CO_2$ injection, and clearly demonstrate that injecting $N_2$ can reverse these changes.
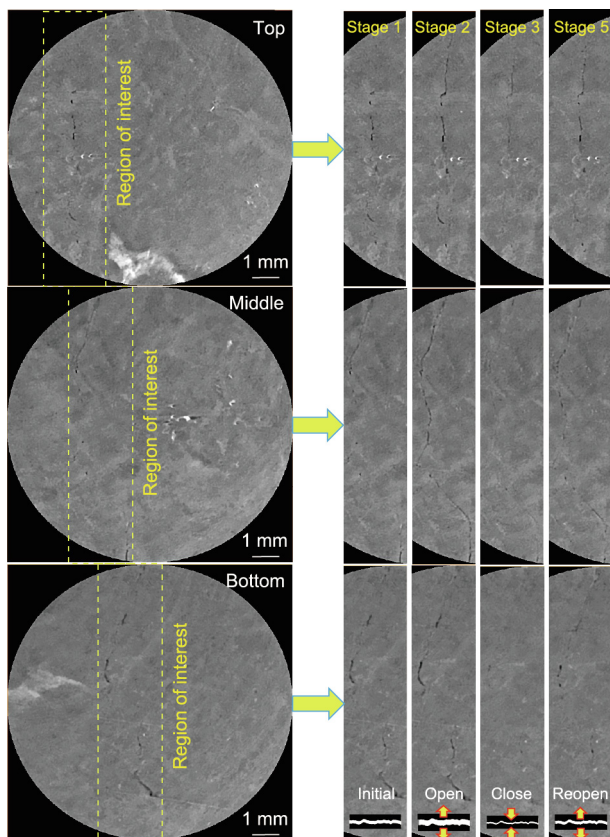


**Fig. 6.** Fracture evolution in representative planes (top, middle, and bottom regions) along the longitudinal direction. CT images in stage 1 (initial), 2 ($N_2$ pre $CO_2$), 3 ($CO_2$), and 5 ($N_2$ after $CO_2$) are compared. In the grayscale CT images, brightness contrasts among various compositions of coal represent the X-ray attenuation of each composition, which mainly depends on the material density. Minerals, organic matter, and fractures are shown in white, grey, and black, respectively. Fractures in the sample are marked by yellow dashed-line boxes.
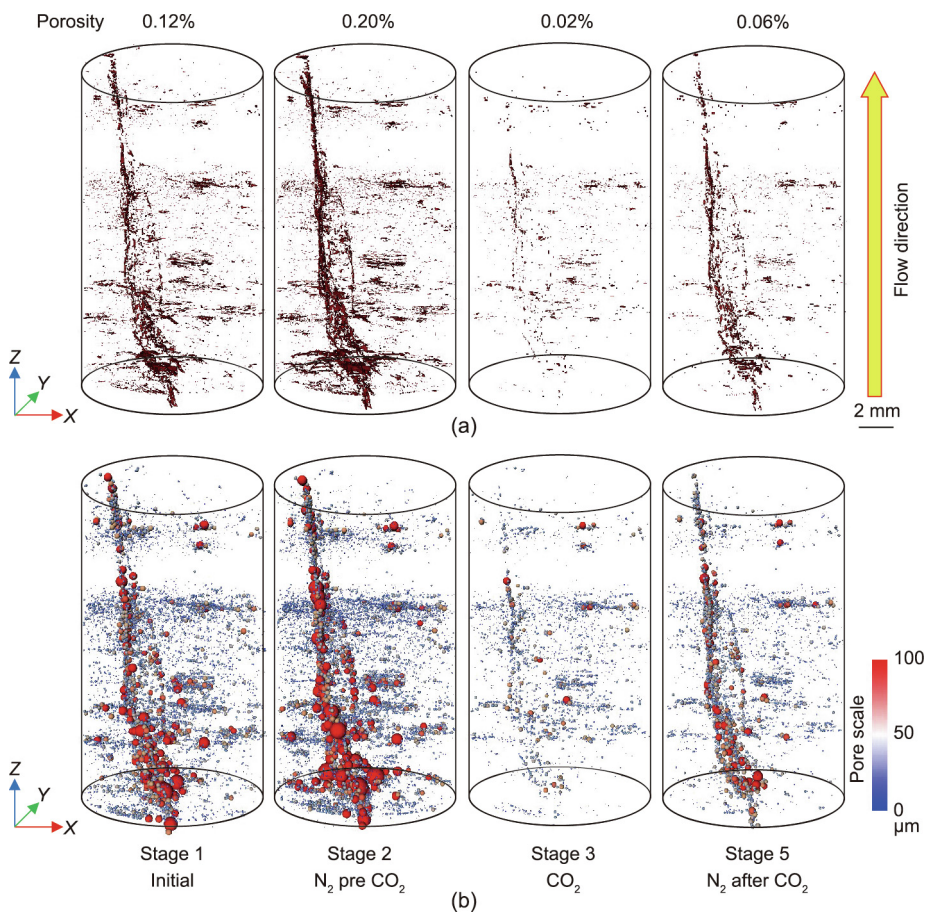
### 3.3. Flue-gas injection for ECBM in deep coal seams

Volume changes of the coal in $CO_2$-ECBM for deep coal seams are of key importance, since coal permeability is affected by these changes; in turn, it affects $CO_2$ injectivity and $CH_4$ production. During the past $CO_2$-ECBM field projects for deep coal seams, the operators had to reduce the injection rates after a certain period of $CO_2$ injection due to an unexpected pressure increase at the injection well. In this study, we directly demonstrate that the experienced injectivity loss can be attributed to a decrease of coal permeability caused by coal swelling.

Our results suggest that injecting $N_2$ can reverse the lost permeability by reopening the fracture network that has closed from

**Fig. 7.** (a) 3D fracture network evolution and (b) equivalent pore network models (diameter: 10.5 mm; height: 18 mm).
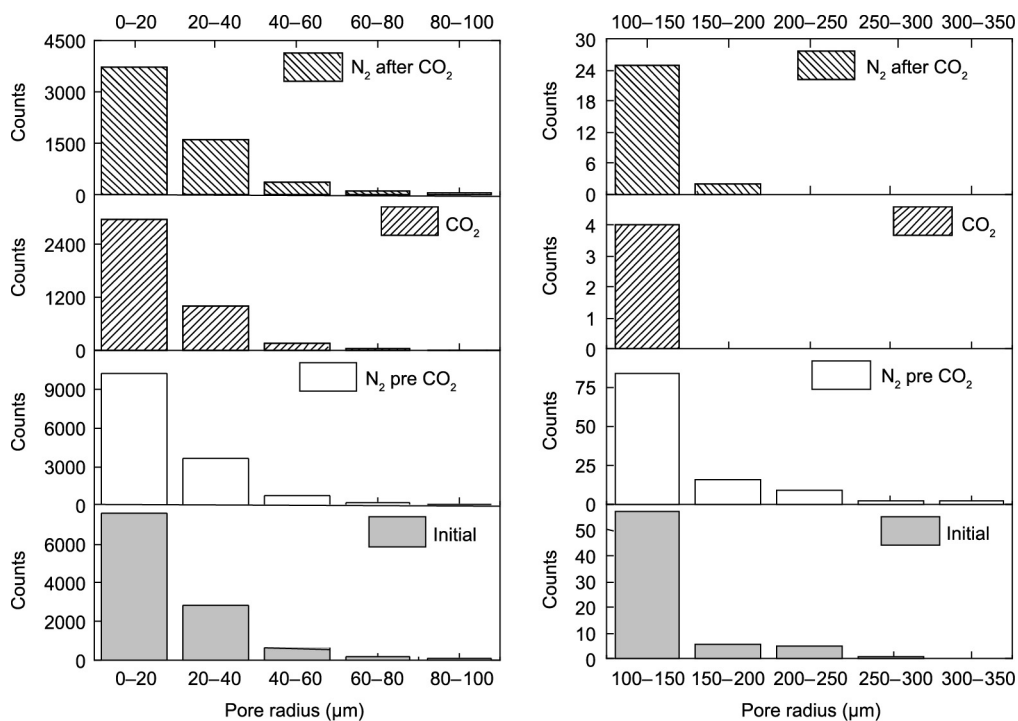


**Fig. 8.** Pore-size distributions.

**Table 2**
Pore numbers and sizes.

| Condition | Total No. | Min radius (μm) | Max radius (μm) | Avg radius (μm) | Percentage of large pores (>100 μm) |
|---|---|---|---|---|---|
| Initial | 11 323 | 9.1 | 272.0 | 20.5 | 41.7% |
| $N_2$ pre $CO_2$ | 15 049 | 9.1 | 327.2 | 20.2 | 55.2% |
| $CO_2$ | 4 194 | 9.1 | 117.1 | 18.2 | 7.1% |
| $N_2$ after $CO_2$ | 5 980 | 9.1 | 170.3 | 21.6 | 22.2% |

No.: number; Min: minimum; Max: maximum; Avg: average.

matrix swelling induced by past $CO_2$ adsorption. Indeed, the $N_2$ flooding test in the field project of the Ishikari Coal Basin of Japan showed that the daily $CO_2$ injection rate was boosted (up to four-fold) by the $N_2$ injection, albeit only temporarily [22]. Therefore, in order to maintain permeability, an alternative could be adopted: injecting either $CO_2$-alternating-$N_2$ or flue gas (a mixture of mainly $N_2$ and $CO_2$). It is encouraging that injecting flue gas (13% $CO_2$ and 87% $N_2$) and synthetic flue gas (47% $CO_2$ and 53% $N_2$) in Alberta, Canada—the world's first flue-gas ECBM pilot project—did not result in reports of swelling and injectivity loss [40,41]. Numerical studies have shown that a collaboration between $CO_2$ and $N_2$ in the injected mixture results in a larger $CH_4$ production rate, which has a $CO_2$ sequestration ability similar to that of a pure $CO_2$-injected ECBM recovery process [42]. The optimum ratio of $N_2$ and $CO_2$ in the injection gas depends on the technical and commercial requirements. In flue-gas injection, ECBM is controlled by two distinct mechanisms: ① The partial pressure of methane is reduced by introducing $N_2$ as a low adsorbing gas; and ② methane is directly displaced from the coal matrix by introducing $CO_2$ as a strong adsorbing gas. The higher the $CO_2$ ratio in the injection gas, the more $CO_2$ can be sequestrated—yet the more swelling and permeability loss can be caused. $N_2$ injection can help maintain adequate permeability (>1 mD by estimate [13,43]), while leading to more rapid methane recovery compared with $CO_2$ injection. Overall, we expect that an optimum mix of $CO_2$ and $N_2$ will compromise between commercial and sequestration aspects, and will also depend on the reservoir properties (e.g., permeability) and operational parameters (e.g., injection pressure and injection-well arrangement).

$CO_2$ concentrations are typically around 10%–15% by volume in power-plant flue gas [44]. With minimal treatment, the flue gas being used for ECBM can come directly from the power stations in the same areas. The byproduct produced from flue-gas-ECBM—namely, $CH_4$—can also be used as an alternative fuel for these power stations. However, the early nitrogen breakthrough may lower the purity of the methane produced, resulting in the need for additional gas separation before use. Because the cost of CCS is dominated by the cost of capture and gas separation (about three-fourths of the total cost [45]), the overall cost could be lowered substantially by injecting gas mixtures (i.e., flue gas) rather than pure $CO_2$. Based on the production economics analysis for the Alberta pilot project [46,47], flue-gas-ECBM is more economical than $CO_2$-ECBM, requiring an approximately 50% wellhead coalbed methane (CBM) price in order to break even. The results of the economic analysis will change, depending on the day's gas prices and $CO_2$ cost. Advances in ECBM technology (e.g., increased injectivity) and government incentives would improve the economics of coalbed sequestration. On the other hand, certain operational constraints, such as increased gas compression costs due to the addition of $N_2$ and the lower purity of $CH_4$ produced after early $N_2$ breakthrough, also need to be considered in the project design.

## 4. Conclusions

The uptake and release of $CO_2$ as an adsorbing gas is associated with the swelling and shrinkage of coal, respectively. The perme-

ability reduction phenomenon has been experienced in several $CO_2$-ECBM field projects and many laboratory experiments across the world in past decades. We directly observed and quantified these phenomena using *in situ* synchrotron X-ray phase-contrast microtomography. The utilization of a three-dimensional (3D) visualization technique allowed us to see the swelling/shrinkage of coal due to $CO_2/N_2$ injection under confinement. Our results confirm that coal does indeed swell when exposed to $CO_2$, due to its adsorbing nature. In contrast, coal undergoes shrinkage upon exposure to $N_2$ because, as a relatively inert gas, $N_2$ lowers the partial pressure and causes $CO_2$ desorption. The results of this study indicate that flue-gas injection is an attractive option for ECBM in deep coal seams in terms of both technical and economic aspects. Firstly, compared with pure $CO_2$ injection, injecting flue gas directly skips the expensive $CO_2$ capture process, while simultaneously maintaining the permeability at a high enough level for long-term gas injection and methane production. Secondly, it allows $CO_2$ storage in coal seams as an added value compared with pure $N_2$ injection. The results of this study have not yet been implemented on a reservoir scale, but they provide the microscale mechanisms. Determining whether flue-gas injection for ECBM in deep coal seams is indeed possible requires more research work and pilot tests under various geological conditions.

## Acknowledgments

## Authors' contribution

P.G. Ranjith supervised the project. Guanglei Zhang performed the experiments, analyzed the data, and wrote the manuscript. Herbert E. Huppert and P.G. Ranjith reviewed and edited the manuscript.

## Compliance with ethics guidelines

Guanglei Zhang, P.G. Ranjith, and Herbert E. Huppert declare that they have no conflict of interest or financial conflicts to disclose.

## References

[1] Keeling. The Keeling Curve [Internet]. 2020 [cited 2020 Mar 13]. Available from: https://scripps.ucsd.edu/programs/keelingcurve/.

[2] IPCC. Global Warming of 1.5 °C. An IPCC Special Report on the impacts of global warming of 1.5 °C above pre-industrial levels and related global greenhouse gas emission pathways, in the context of strengthening the global response to

† https://www.massive.org.au.

the threat of climate change, sustainable development, and efforts to eradicate poverty. Report: IPCC; 2018.

[3] Bickle MJ. Geological carbon storage. Nat Geosci 2009;2(12):815–8.

[4] Huppert HE, Neufeld JA. The fluid mechanics of carbon dioxide sequestration. Annu Rev Fluid Mech 2014;46(1):255–72.

[5] IPCC. IPCC special report on carbon dioxide capture and storage. In: Metz B, Davidson O, de Coninck HC, Loos M, Meyer LA, editors. Prepared by Working Group III of the Intergovernmental Panel on Climate Change. IPCC; 2005.

[6] Bui M, Adjiman CS, Bardow A, Anthony EJ, Boston A, Brown S, et al. Carbon capture and storage (CCS): the way forward. Energy Environ Sci 2018;11 (5):1062–176.

[7] Boot-Handford ME, Abanades JC, Anthony EJ, Blunt MJ, Brandani S, Mac Dowell N, et al. Carbon capture and storage update. Energy Environ Sci 2014;7 (1):130–89.

[8] IEA. Technology Roadmap: carbon capture and storage Report. Paris: International Energy Agency; 2013.

[9] Cook PJ editor Geologically storing carbon: learning from the Otway Project experience. Collingwood: CSIRO Publishing; 2014.

[10] Metz B, Davidson O, de Coninck H, Loos M, Meyer L. IPCC special report on carbon dioxide capture and storage. Report. Geneva: Intergovernmental Panel on Climate Change: 2005 Sep.

[11] Liu Y, Rui Z, Yang T, Dindoruk B. Using propanol as an additive to $CO_2$ for improving $CO_2$ utilization and storage in oil reservoirs. Appl Energy 2022;311:118640.

[12] Liu Y, Rui Z. A storage-driven $CO_2$ EOR for net-zero emission target. Engineering. In press.

[13] White CM, Smith DH, Jones KL, Goodman AL, Jikich SA, LaCount RB, et al. Sequestration of carbon dioxide in coal with enhanced coalbed methane recovery a review. Energy Fuels 2005;19(3):659–724.

[14] Mukherjee M, Misra S. A review of experimental research on Enhanced Coal Bed Methane (ECBM) recovery via $CO_2$ sequestration. Earth Sci Rev 2018;179:392–410.

[15] Harpalani S, Prusty BK, Dutta P. Methane/$CO_2$ sorption modeling for coalbed methane production and $CO_2$ sequestration. Energy Fuels 2006;20 (4):1591–9.

[16] Godec M, Koperna G, Gale J. $CO_2$-ECBM: a review of its status and global potential. Energy Procedia 2014;63:5858–69.

[17] Fulton PF, Parente CA, Rogers BA, Shah N, Reznik A. A laboratory investigation of enhanced recovery of methane from coal by carbon dioxide injection. In: Proceedings of the SPE Unconventional Gas Recovery Symposium; 1980 May 18–21; Pittsburgh, PA, USA. Richardson: OnePetro; 1980.

[18] Reznik AA, Singh PK, Foley WL. An analysis of the effect of $CO_2$ injection on the recovery of *in situ* methane from bituminous coal: an experimental simulation. Soc Pet Eng J 1984;24(05):521–8.

[19] Gunter WD, Gentzis T, Rottenfusser BA, Richardson R. Deep coalbed methane in Alberta, Canada: a fuel resource with the potential of zero greenhouse gas emissions. Energy Convers Manage 1997;38:S217–22.

[20] Stevens SH, Spector D, Riemer P. Enhanced coalbed methane recovery using $CO_2$ injection: worldwide resource and $CO_2$ sequestration potential. In: Proceedings of the SPE International Oil and Gas Conference and Exhibition in China; 1998 Nov 2–6; Beijing, China. Richardson: OnePetro; 1998.

[21] Pan Z, Ye J, Zhou F, Tan Y, Connell LD, Fan J. $CO_2$ storage in coal to enhance coalbed methane recovery: a review of field experiments in China. Int Geol Rev 2018;60(5–6):754–76.

[22] Fujioka M, Yamaguchi S, Nako M. $CO_2$-ECBM field tests in the Ishikari Coal Basin of Japan. Int J Coal Geol 2010;82(3–4):287–98.

[23] Wong S, Law D, Deng X, Robinson J, Kadatz B, Gunter WD, et al. Enhanced coalbed methane and $CO_2$ storage in anthracitic coals—micro-pilot test at south Qinshui, Shanxi, China. Int J Greenh Gas Control 2007;1(2):215–22.

[24] van Bergen F, Pagnier H, Krzystolik P. Field experiment of enhanced coalbed methane-$CO_2$ in the upper Silesian basin of Poland. Environ Geosci 2006;13 (3):201–24.

[25] Reeves SR. The Coal-Seq project: key results from field, laboratory, and modeling studies. In: Rubin ES, Keith DW, Gilboy CF, Wilson M, Morris T, Gale J, Thambimuthu K, editors. the 7th International Conference on Greenhouse Gas Control Technologies; 2004 Sep; Vancouver, Canada. Amsterdam: Elsevier; 2004. p. 1399–403.

[26] Fokker PA, van der Meer LGH. The injectivity of coalbed $CO_2$ injection wells. Energy 2004;29(9–10):1423–9.

[27] Karacan CÖ. Heterogeneous sorption and swelling in a confined and stressed coal during $CO_2$ injection. Energy Fuels 2003;17(6):1595–608.

[28] Walker Jr PL, Verma SK, Rivera-Utrilla J, Khan MR. A direct measurement of expansion in coals and macerals induced by carbon dioxide and methanol. Fuel 1988;67(5):719–26.

[29] Zhang X, Ranjith PG, Li D, Perera MSA, Ranathunga AS, Zhang B. $CO_2$ enhanced flow characteristics of naturally-fractured bituminous coals with $N_2$ injection at different reservoir depths. J $CO_2$ Util 2018;28:393–402.

[30] Kiyama T, Nishimoto S, Fujioka M, Xue Z, Ishijima Y, Pan Z, et al. Coal swelling strain and permeability change with injecting liquid/supercritical $CO_2$ and $N_2$ at stress-constrained conditions. Int J Coal Geol 2011;85(1):56–64.

[31] Zhang G, Ranjith PG, Wu B, Perera MSA, Haque A, Li D. Synchrotron X-ray tomographic characterization of microstructural evolution in coal due to supercritical $CO_2$ injection at *in-situ* conditions. Fuel 2019;255:115696.

[32] Zhang G, Ranjith PG, Liang W, Haque A, Perera MSA, Li D. Stress-dependent fracture porosity and permeability of fractured coal: an *in-situ* X-ray tomography study. Int J Coal Geol 2019;213:103279.

[33] Zhang B, Liang W, Ranjith PG, Li Z, Li C, Hou D. Coupling effects of supercritical $CO_2$ sequestration in deep coal seam. Energy Fuels 2019;33(1):460–73.

[34] Orr Jr FM. Onshore geologic storage of $CO_2$. Science 2009;325(5948):1656–8.

[35] Brace WF, Walsh J, Frangos WT. Permeability of granite under high pressure. J Geophys Res 1968;73(6):2225–36.

[36] Heller R, Vermylen J, Zoback M. Experimental investigation of matrix permeability of gas shales. AAPG Bull 2014;98(5):975–95.

[37] Mayo SC, Gureyev TE, Nesterets YI, Thompson DA, Siu KKW, Wallwork K. A dedicated micro-CT beamline for the Australian Synchrotron and the Remote-CT project. J Phys: Conf Ser 2013;463:012002.

[38] Zhang G, Ranjith PG, Perera MSA, Haque A, Choi X, Sampath KSM. Characterization of coal porosity and permeability evolution by demineralisation using image processing techniques: a micro-computed tomography study. J Nat Gas Sci Eng 2018;56:384–96.

[39] Youssef S, Rosenberg E, Gland NF, Kenter JA, Skalinski M, Vizika O, et al. High resolution CT and pore-network models to assess petrophysical properties of homogeneous and heterogeneous carbonates. In: Proceedings of the SPE/EAGE Reservoir Characterization and Simulation Conference; 2007 Oct 28–31; Abu Dhabi, UAE. Richardson: OnePetro; 2007.

[40] Gunter W. Coalbed methane, a fossil fuel resource with the potential for zero greenhouse gas emissions—the Alberta, Canada Program 1996–2009: a summary. Alberta $CO_2$-ECBM research and field pilots summary. Alberta Research Council; 2009.

[41] Mavor MJ, Gunter WD, Robinson JR. Alberta multiwell micro-pilot testing for CBM properties, enhanced methane recovery and $CO_2$ storage potential. In: Proceedings of the SPE Annual Technical Conference and Exhibition; 2004 Sep 26–29; Houston, Texas, USA. Richardson: OnePetro; 2004.

[42] Talapatra A, Halder S, Chowdhury AI. Enhancing coal bed methane recovery: using injection of nitrogen and carbon dioxide mixture. Petrol Sci Technol 2021;39(2):49–62.

[43] Stevens SH, Kuuskraa VA, Gale J, Beecy D. $CO_2$ injection and sequestration in depleted oil and gas fields and deep coal seams: worldwide potential and costs. Environ Geosci 2001;8(3):200–9.

[44] Davis SJ, Lewis NS, Shaner M, Aggarwal S, Arent D, Azevedo IL, et al. Net-zero emissions energy systems. Science 2018;360(6396):eaas9793.

[45] Xu X, Song C, Wincek R, Andresen JM, Miller BG, Scaroni AW. Separation of $CO_2$ from power plant flue gas using a novel $CO_2$ "molecular basket" adsorbent. Fuel Chem Div Prepr 2003;48(1):162–3.

[46] Wong S, Gunter W, Mavor M. Economics of $CO_2$ sequestration in coalbed methane reservoirs. In: Proceedings of the SPE/CERI Gas Technology Symposium; 2000 Apr 3–5; Calgary, Alberta, Canada. Richardson: OnePetro; 2000.

[47] Wong S, Gunter W, Law D, Mavor M. Economics of flue gas injection and $CO_2$ sequestration in coalbed methane reservoirs. In: Williams D, Durie B, McMullan P, Paulson C Smith, A, editors. In: Proceedings of the 5th International Conference on Greenhouse Gas Control Technologies. Cairns: CSIRO Publishing; 2001. p. 543–8.